Hindawi
International Journal of Energy Research
Volume 2023, Article ID 9979610, 19 pages
https://doi.org/10.1155/2023/9979610

*Research Article*

# Stochastic Unit Commitment Study in a Power System with Flexible Load in Presence of High Penetration Renewable Farms

**Mostafa Mojtahedzadeh Larijani**,[1] **Mehrdad Ahmadi Kamarposhti**,[2] **and Tohid Nouri**[1]

[1]*Department of Electrical Engineering, Sari Branch, Islamic Azad University, Sari, Iran*
[2]*Department of Electrical Engineering, Jouybar Branch, Islamic Azad University, Jouybar, Iran*

Correspondence should be addressed to Mehrdad Ahmadi Kamarposhti; mehrdad.ahmadi.k@gmail.com

Received 20 March 2023; Revised 31 May 2023; Accepted 8 June 2023; Published 7 July 2023

Academic Editor: Yashwant Sawle



In this paper, a new hybrid multiobjective algorithm, namely, the modified bald eagle search Algorithm (MBES), integrated with the grasshopper optimization algorithm, is proposed to solve the unit commitment (UC) problem. We consider a standard 10-unit power system with two wind farms, two photovoltaic farms, and flexible loads for optimization purposes. The UC problem is tackled under uncertainties related to demand and renewable generation capacities. To account for these uncertainties, probability density functions (PDFs) are assigned to the sources of uncertainty, and Monte Carlo simulation (MCS) is employed to select several scenarios with specific probability coefficients. Additionally, two innovative objective functions based on operation cost and emissions are introduced, with each scenario weighted based on its occurrence probability. To assess the performance of the proposed MOGOA-MBES algorithm, simulations are conducted across three scenarios with varying conditions, and the results are compared against those obtained from several multiobjective algorithms. Our findings, supported by optimization results and the S-metric index, demonstrate that the proposed MOGOA-MBES algorithm outperforms other algorithms in terms of reducing operation cost and emissions. Furthermore, the simulation results reveal that uncertainties lead to an increase in cost and emissions, whereas the inclusion of flexible loads and their participation in the UC program can effectively mitigate cost and emission levels.

## 1. Introduction

One of the important and fundamental issues in the power system study is providing the electrical demand for consumers at a lower operating cost. Certainly, it cannot be done in any way, and there are many limitations [1, 2]. Therefore, unit commitment (UC) is one of the most important subjects in power system operation [3]. In recent decades, due to the increase in the price of energy as well as environmental emission, the use of renewable energy sources such as wind and photovoltaic farms has increased [4]. If the penetration of these resources increases, they can directly affect the studies of economic dispatch (ED) and unit commitment directly, and the power system calculations will change [5, 6]. On the other hand, uncertainty is an undeniable part of systems analysis. Without considering uncertainty, the results do not have sufficient validity and accuracy [7]. In recent years, several studies have been done in the field of unit commitment of the power system to renewable sources [8–10]. Unit UC studies can be divided into six categories: traditional methods [11], innovative methods [12], artificial intelligence methods [13–15], stochastic methods [16], estimated control methods [17], and other theoretical methods [18].

The traditional methods used in the UC program include linear programming (LP) [19], nonlinear programming (NLP) [20] and law-based methods of dynamic programming [21]. In [22], a UC program is done based on the on/off mode of power generation units and the continuous implementation of power sharing. Also, mixed integer linear programming (MILP) is used to solve the UC problem and minimizing

operation cost. In [23], the MILP is used for solving the UC problem, and the demand response program (DRP) is used to reduce peak hour load. The results show that DRP can help reduce operation cost. Traditional methods cannot be the best solution for the UC problem because they are not practical due to the nonlinearity and high order of power systems. In recent years, metaheuristic algorithm are used for solving UC problem. The optimization algorithms such as whale optimization algorithm (WOA) [24], genetic algorithm (GA) [25], particle swarm optimization (PSO) algorithm [26], and gray wolf optimization (GWO) algorithm [27]. Bayesian optimization is also used for unit commitment and reducing cost and emission in the power system [28]. Bayesian optimization is an effective approach for fixing luxurious black-box optimization issues, and it determines the candidates' answers for steeply priced evaluation via optimizing the acquisition characteristic [29]. In [30], a parameter-free self-tuning variant of NSGA-II for multiobjective environmental/economic dispatch optimization. NSGA-RL outperforms NSGA-II and other existing methods, achieving improved satisfaction levels and a well-distributed Pareto front. It eliminates the need for parameter tuning, making it a promising approach for multiobjective optimization problems. In [31], a binary fish migration algorithm is proposed for solving the UC problem. The UC model for this reference is a combination of thermal units' operation cost, investment cost, and distributed generation cost. Metaheuristic algorithms have a weakness in their dependency on algorithm parameter tuning. Poor selection of algorithm parameters can lead to algorithm nonconvergence or getting trapped in local optima [32].

Including demand response program (DRP) in the UC problem is done in recent years. The participation of flexible loads in DRP can greatly reduce the cost of operating the power system [33]. The flexible loads can reduce their subsumption when the power system faces an energy shortage. Therefore, for the duration and amount of energy reduction by flexible loads in the power system, they should be rewarded. In addition to reducing the power shortage and reducing the operating cost, the presence of flexible loads in the power system is effective in improving the load profile, and improving the power quality and reliability indexes of power systems [34]. In [35], DRP is considered in the UC program, and the operation cost has been reduced by 2.5% compared to the nonimplementation of DRP. Also, a genetic algorithm is used for solving the UC problem.

The weakness of the reviewed articles is not considering uncertainty. Uncertainty is an undeniable part of the UC studies, and considering the uncertainty will increase the accuracy of the UC results. The main source of uncertainty in the UC program for the power system with renewable farm are load uncertainty and renewable generation capacity uncertainty [36]. Also, the price of electricity and load also have uncertainty. The amount of storage power, amount of production, load, and price of electricity in UC are estimated by several methods, and the inherent error of this forecast causes deviation from the optimal plan and, as a result, it causes inappropriate use [37]. On the one hand, changes in weather conditions affect the production of renewable resources, and on the other hand, they change the amount of load. The estimated weather conditions for the participation program of the power generation units are made according to the meteorological data from the local center or the external center [38].

In this paper, the UC program a standard power system in present of photovoltaic and wind farm with high penetration is done. In the UC study, the uncertainties of the electrical load and renewable farms are considered, and a weighted objective function based on scenario possibilities is proposed. So, possible scenarios are more effective in the objective function values due to the increase in their coefficient. Also, an innovative hybrid algorithm of the multiobjective grasshopper optimization algorithm and modified bald eagle search (MOGOA-MBES) is proposed to solve the problem. Therefore, the main contributions of this paper are

(i) Proposing weighted heuristic objective functions based on the probability of occurrence

(ii) Proposing an innovative hybrid algorithm with accuracy

(iii) Solving the problem of the participation of units in the power system with high penetration of renewable PV and wind farms

In Figure 1, the graphical abstract of UC problem solving method is shown.

In the following, problem formulation is done in Section 2. In this section, load and renewable source uncertainty modeling is done first, and then the Monte Carlo simulation for scenario selection is briefly described. Finally, the proposed objective functions and problem constraints are introduced. In Section 3, the proposed hybrid optimization algorithm is introduced. The simulation result analysis is done in Section 4. The results are compared with several algorithms. Finally, the conclusions and suggestions for the future research are done in Section 5.

## 2. Problem Formulation

The unit commitment problem in the presence of uncertainties requires a complete understanding of the influential sources of uncertainty and their accurate and appropriate modeling. In the studied power system, electrical load uncertainty and renewable farm power uncertainty are considered, and other uncertainty sources are ignored due to their small impact on the UC problem. To model the uncertainties, the probability density function (PDF) corresponding to load and generation uncertainties should be carefully selected according to the values of the previous measurements.

*2.1. Uncertainties Modeling.* The electrical demand in the power system constantly changes, and it is not possible to consider an accurate pattern for the load changes. Weather condition changes and time vary are two main factors in changing consumption patterns. Daily and weekly changes in demand mainly depend on the behavior patterns of different energy consumers. Uncertainty created due to changes in loading conditions can have a significant impact on the UC study. Previous studies and applications have shown that the use of the normal distribution aligns well with real-world

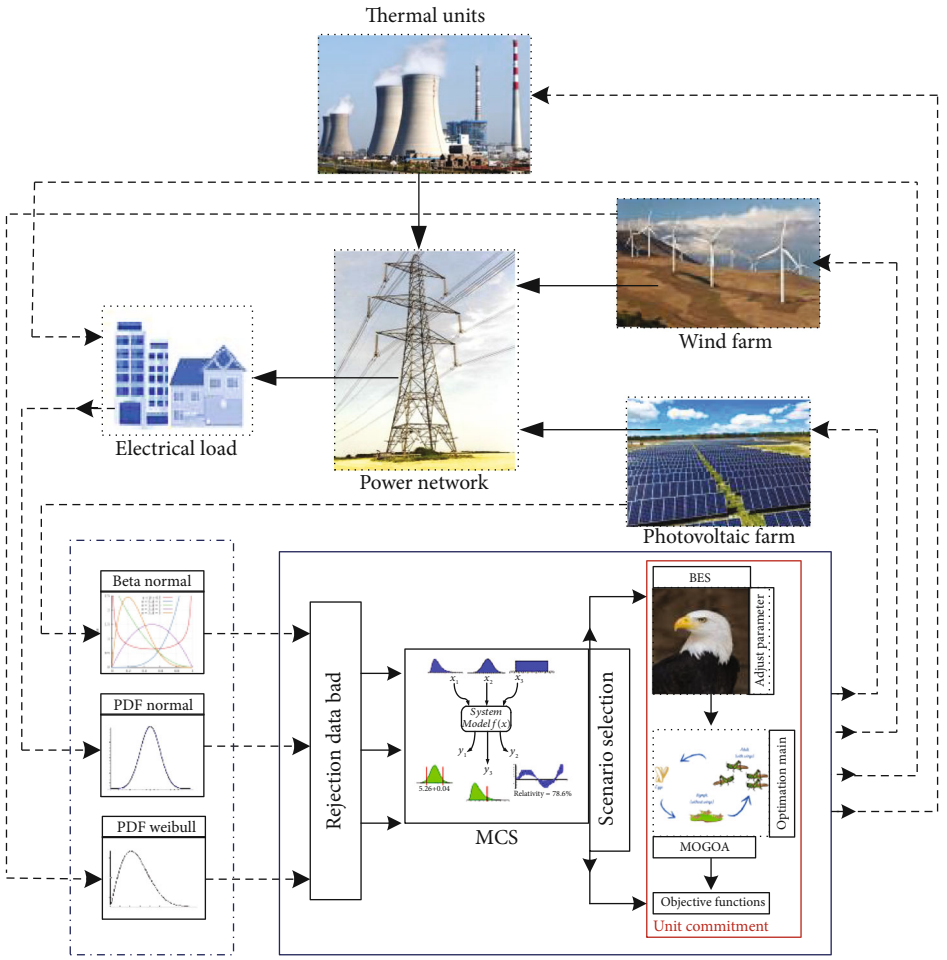


Figure 1: Graphical abstract of the proposed UC problem solving method.

data on electrical load intensity and provides acceptable results. The normal PDF is widely used for electrical demand uncertainty modeling, which can be expressed in the form of equation (1) [39].

$$f(P_L) = \frac{1}{\sqrt{2\pi}^* \sigma_{PL}} \exp\left(-\frac{(P_L - \mu_{PL})^2}{2^* \sigma_{PL}^2}\right), \quad (1)$$

where $P_L$, $\mu_{PL}$, and $\sigma_{PL}$ are electrical load, average load, and standard deviation, respectively. The uncertainty of wind power is studied as another important influencing factor in the problem of UC in the understudy power system. Wind speed is a random variable, and meteorological data can be suitable for estimating the wind energy potential. Wind speeds in many geographical areas exhibit a phenomenon that can be described by the Weibull distribution. The Weibull distribution is defined by two main parameters called shape and scale. These parameters allow for customization of the Weibull distribution to fit the data and describe specific conditions such as gust length, and maximum wind

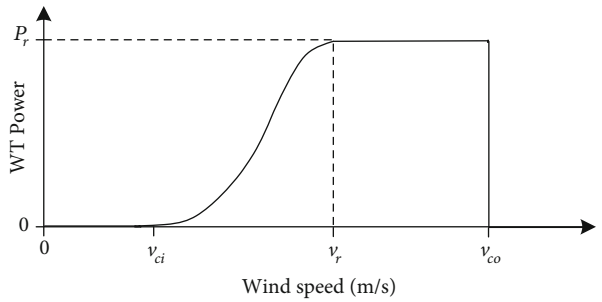


Figure 2: The wind farm power curve.

speed. The probabilistic nature of wind speed can be modeled by the Weibull PDF [40].

$$f_t^{\mathrm{WT}}(v) = \frac{k_t}{c_t} \times \left(\frac{v_t}{c_t}\right)^{k_t - 1} \exp\left(-\left(\frac{v_t}{c_t}\right)^{k_t}\right), \quad \text{for } c_t > 1, k_t > 0, \quad (2)$$

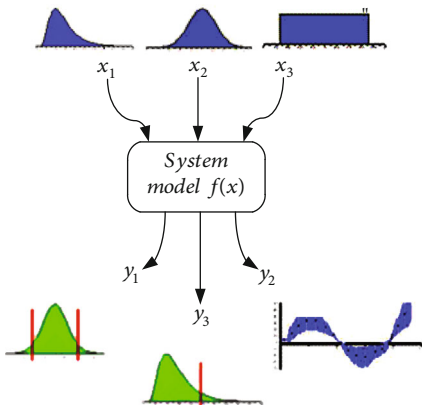


Figure 3: The Monte Carlo method scheme.

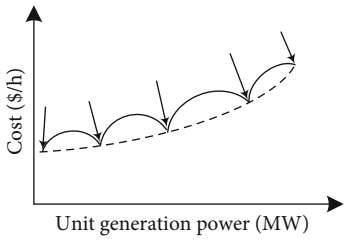


Figure 4: The thermal unit cost.

where $v_t$ is wind speed and $k_t$ and $c_t$ are the shape factor and scale factor of the Weibull PDF which are calculated by

$$k_t = \left(\frac{\sigma_t^v}{\mu_t^v}\right)^{-1.086}, \tag{3}$$

$$C_t = \frac{\mu_t^v}{\Gamma(1+(1/k_t))}, \tag{4}$$

where $\mu_t^v$ and $\sigma_t^v$ are the mean and variance of the wind data, respectively. These parameters are calculated based on historical data of wind speed. The wind farm generation capacity can be calculated by

$$P_w = \begin{cases} P_r \dfrac{V^3 - V_{ci}^3}{V_r^3 - V_{ci}^3}, & V_{ci} \le V \le V_r, \\ P_r, & V_r \le V \le V_{co}, \\ 0, & o.w, \end{cases} \tag{5}$$

where $P_r$ is wind farm rated power, and $V_{ci}$, $V_{co}$, and $V_r$ cut-in, cut-off, and rated wind speeds of wind turbines, respectively. The wind turbine power curve is shown in Figure 2.

The production power of the photovoltaic farm depends on the intensity of solar radiation, the absorption capacity of the array surface, and the ambient temperature. The intensity of solar radiation has a probabilistic nature. Previous studies and simulations have demonstrated that the use of the beta distribution aligns well with observed data on solar radiation intensity. The beta distribution is defined by two primary parameters, called alpha and beta. Estimating these

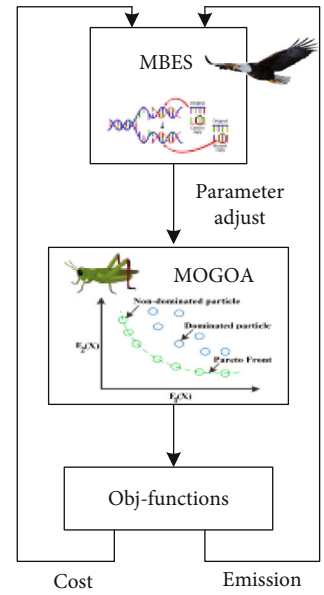


Figure 5: The proposed MOGOA-MBES mechanism.

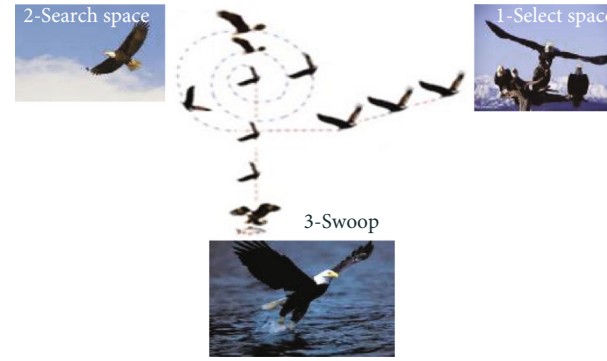


Figure 6: The bald eagle hunting steps.

parameters from observed data is relatively straightforward and can be performed using common statistical inference methods. Beta PDF can be used to estimate the solar radiation on the farm which is formulated by equation (6) [41].

$$f_{\mathrm{pv}}^t(\mathrm{si}^t) = \begin{cases} 0, & \alpha^t > 0, \beta^t > 0, \\ \dfrac{\Gamma(\alpha^t + \beta^t)}{\Gamma(\alpha^t)\Gamma(\beta^t)} (\mathrm{si}^t)^{\alpha^t - 1} (1 - \mathrm{si}^t)^{\beta^t - 1}, & o.w, \end{cases} \tag{6}$$

where $\mathrm{si}^t$ is irradiation random variable, $\Gamma$ is gamma function, $\alpha^t$ and $\beta^t$ are the parameters of the beta PDF. The values of $\alpha^t$ and $\beta^t$ depend on the mean and standard deviation of the radiation data. The PV farm generation capacity can be calculated by equation (23)

$$P_{PV} = P_r \times f_{PV}\left(\frac{\mathrm{si}}{\mathrm{si}_s} + \alpha_t(T - T_s)\right), \tag{7}$$

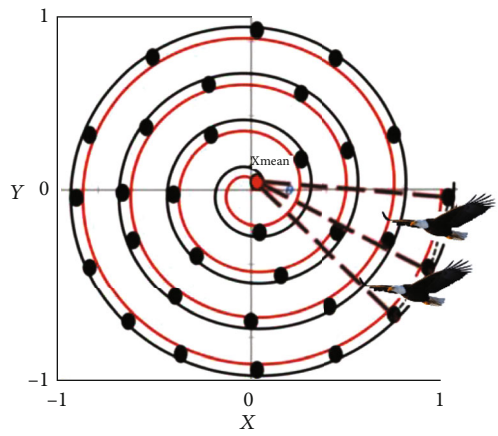


Figure 7: Bald eagles search stage and spiral movement.

where $P_r$ is photovoltaic farm rated power, $f_{PV}$ is photovoltaic array surface cleanliness factor, $si_s$ is standard irradiation (1000 w/m$^2$), $\alpha_t$ temperature coefficient, $T$ is array temperature, and $T_s$ is standard temperature (25°C).

*2.2. Scenario Generation.* To consider the uncertainty related to variables, the iterative technique is used. The problem is solved in several times and each time, the possible input variables are selected using the probability density function. In this method, a stopping criterion is defined to ensure that the correct result is obtained. The stopping criterion is a criterion that, if it is fulfilled in every iteration of solving the problem, the problem ends and the obtained results are displayed in the output. In the framework of probabilistic analysis of the objective function, the problem is expressed as $y = f(z)$, where $z$ is the vector of possible variables of the problem, and the dense function has a unique probability. In this case, for the possible analysis of the problem, the objective function is calculated in the form of

$$y = \sum_{s=1}^{N_s} \pi_s \times f(z), \tag{8}$$

where $\pi_s$ is the $s$th scenario possibility, and $f$ is its fitness. The value of $\pi_s$ in each scenario is determined by the probability density function. The Monte Carlo simulation (MCS) method is also used to select the scenario. The scattering of scenarios selected by MCS helps to select the most likely conditions that may occur in the power system. In Figure 3, an overview of the Monte Carlo method is shown.

The fundamental steps of uncertainty calculation by the Monte Carlo method are as follows:

*Step 1*: definition of the mathematical model of the measurement system

*Step 2*: select PDF for each input quantities

*Step 3*: obtaining the probability density functions of the output quantity

*Step 4*: determining the uncertainty of the measurement system

*2.3. Objective Functions.* To solve the UC problem, two objective functions are considered. The first objective function is defined based on operation cost, and the second objective function is defined based on environmental emission. The operation cost function is a combination of the power generation cost of power plant units, wind and photovoltaic farm costs, transmission losses cost, and the cost of flexible loads by participating in the demand response program.

$$\begin{aligned}\operatorname{Min} f_1 &= \operatorname{Min} \sum_{k=1}^{N_S} S_\kappa \sum_{t=1}^{T} \operatorname{cost}(t) \\ &= \operatorname{Min} \sum_{k=1}^{N_K} S_\kappa \sum_{t=1}^{T} \left( \sum_{u=1}^{N_u} C_U^k(t) + \sum_{i=1}^{N_{wt}} C_{\mathrm{WT}}^i(t) + \sum_{j=1}^{N_{PV}} C_{\mathrm{PV}}^j(t) + C_{\mathrm{Loss}}(t) + C_{\mathrm{DR}}(t) \right),\end{aligned} \tag{9}$$

where $C_U^k(t)$, $C_{\mathrm{WT}}^i(t)$, $C_{\mathrm{PV}}^j(t)$, $C_{\mathrm{Loss}}(t)$, and $C_{\mathrm{DR}}(t)$ are the thermal unit cost, wind farm cost, photovoltaic farm cost, transmission losses cost, and demand response program cost of flexible loads. Also, $S_\kappa$ is the probability of $k$th scenario. The thermal units' cost can be calculated by equation (10) [22].

$$C_U(i,t) = C_U^F(i,t) + C_U^{SC}(i,t), \tag{10}$$

where $C_U^F(i,t)$ is fuel cost of the unit and $C_U^{SC}(i,t)$ is startup and shutdown cost $i$th thermal unit. The fuel cost with considering valve point effect can be calculated by equation (11). The valve point effect in cost function is calculated by sinusoidal term.

$$C_U^F(i,t) = a_i P^2(i,t) + b_i P(i,t) + c_i + \left| d_i \sin\left( e_i \left( P_{\min\,(i)} - P(i,t) \right) \right) \right|. \tag{11}$$

The fuel cost is shown in Figure 4.

The thermal unit startup and shutdown cost can be calculated by

$$C_U^{SC}(i,t) = SUC(i) \times |(U(i,t) - U(i,t-1)|, \tag{12}$$

where each time startup and shutdown (SUC) is calculated by equation (13) according to the duration of the unit being out of service.

$$\mathrm{SUC}(i) = \begin{cases} \mathrm{HSC}(i), & T_{\mathrm{off}} \le \mathrm{CST}(i) + \mathrm{MDT}(i), \\ \mathrm{CSC}(i), & T_{\mathrm{off}} > \mathrm{CST}(i) + \mathrm{MDT}(i), \end{cases} \tag{13}$$

where HSC is the hot startup cost and CSC is cold startup cost. Also, $T_{\mathrm{off}}$ is unit shutdown time interval, CST(i) the time required for cold startup, and MDT(i) is the minimum turn-off time of *i th* unit. The wind farm and PV farm costs are by equations (14) and (15), respectively. It should be noted that the first-order model can be the best choice for renewable farms operation cost, and higher-order equations may cause the complexity of the problem and does not have much effect on the accuracy of the final result and may cause the algorithm to be trapped in the local optimum use of higher order equations will cause the complexity of the problem and does not have much effect on the accuracy of

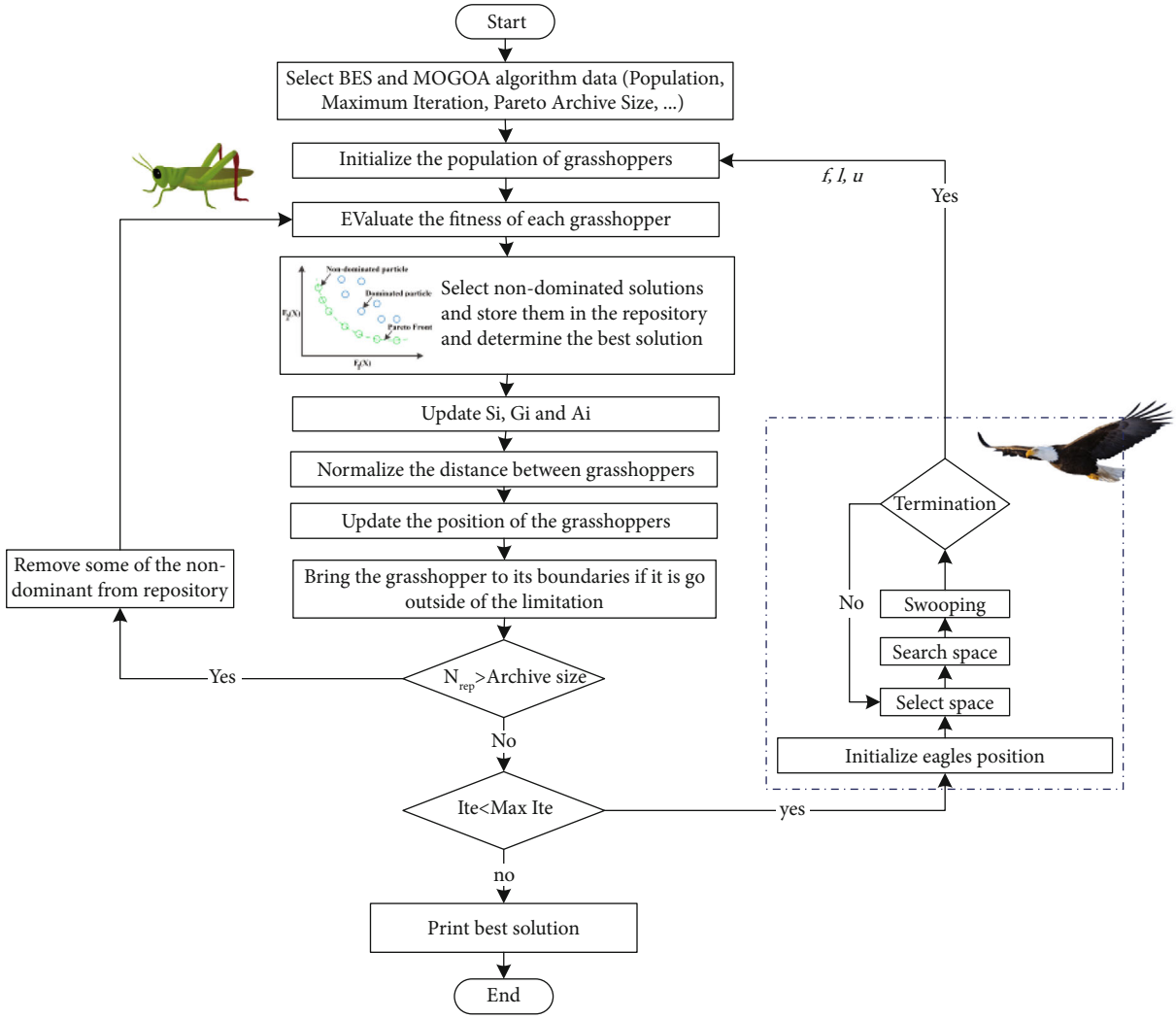


Figure 8: The MOGOA-MBES flowchart.

the final answer and may cause the algorithm to be trapped in the local optimum [24].

$$C^i_{\mathrm{WT}}(t) = A + BP_{\mathrm{wt}}(t), \tag{14}$$

$$C^j_{\mathrm{PV}}(t) = C + DP_{\mathrm{PV}}(t), \tag{15}$$

where A, B, C, and D are the cost coefficients of wind and PV farms, $P_{\mathrm{wt}}(t)$ is generated power of the wind farm, and $P_{\mathrm{PV}}(t)$ is the generated power of the PV farm. The transmission loss cost can be calculated by equation (16) [25].

$$C^E_{\mathrm{Loss}}(t) = P_{\mathrm{Loss}}(t) \times C_E(t), \tag{16}$$

where $P_{\mathrm{Loss}}(t)$ is per hour transmission loss and $C_E(t)$ is electricity price. The $P_{\mathrm{Loss}}(t)$ is calculated using the

$$P_{\mathrm{Loss}} = B_{oo} + \sum_{j=1}^{N_g} B_{jo}P_j + \sum_{i=1}^{N_g}\sum_{j=1}^{N_g} P_iB_{ij}P_j. \tag{17}$$

The UC problem changes if flexible load inn power system is allowed to participate in demand response program (DRP). The reward that should be paid due to the participation of flexible loads in the DRP is calculated by

$$C_{\mathrm{DR}}(t) = P_{\mathrm{DR}}(t) \times R_{\mathrm{DR}}(t), \tag{18}$$

where $P_{\mathrm{DR}}$ is the amount of power reduced by the flexible loads and $R_{\mathrm{DR}}$ is the amount of bonus that is paid to the flexible load for each megawatt of reduced power consumption.

In recent years, governmental and nongovernmental organizations have paid attention to the issue of environmental emission caused by thermal power plant units. Because they believe that a significant share of emissions is related to the power generation units in the power plant. Therefore, in this paper, emission is considered as a separate objective function. The second objective function can be calculated by

$$\mathrm{Min}\, f_2(X) = \mathrm{Min}\sum_{k=1}^{N_S} S_k \sum_{t=1}^{T} \mathrm{Emission}(t) = \mathrm{Min}\sum_{k=1}^{N_S} s_k \sum_{t=1}^{T}\left\{\sum_{k=1}^{N_u} P^k_u(t) \times E^k_u\right\}. \tag{19}$$

**Start**
- •Select the MOGOA-MBES algorithm parameters (Population size, Maximum iteration and etc.)
- •Initialize the MBES population. (Select *f*, *l*, *u*)
- •**While** Ite<Max_Ite
- •**For all** BES **do**
- •Initialize the MOGOA population.
- •Calculate objective function for all the grasshoppers.
- •Find non-dominated particles and store in repository.
- •Select best solution.
- •**While** Ite<Max_Ite
- •**For all** grasshopper **do**
- •Update S, G, A.
- •Update grasshopper position.
- •Find non-dominated particles and update repository.
- •Select best solution.
  **end for**
- •Ite=Ite+1;
- •**end while**
- •perform select space
- •perform search space
- •perform swooping
- •**end for**
- •**end while**

**End**

Algorithm 1: Pseudo-code of the MOGOA-MBES.

Table 1: Cost and emission coefficients of thermal units [69].

| Unit | G1 | G2 | G3 | G4 | G5 | G6 | G7 | G8 | G9 | G10 |
|---|---|---|---|---|---|---|---|---|---|---|
| $p^{\min}$(MW) | 150 | 135 | 73 | 60 | 73 | 57 | 20 | 47 | 20 | 55 |
| $p^{\max}$(MW) | 470 | 460 | 340 | 300 | 243 | 160 | 130 | 120 | 80 | 55 |
| MUT (h) | 8 | 8 | 5 | 5 | 6 | 3 | 3 | 1 | 1 | 1 |
| MDT (h) | 8 | 8 | 5 | 5 | 6 | 3 | 3 | 1 | 1 | 1 |
| Startup cost (cold) ($) | 9000 | 10000 | 1100 | 1120 | 1800 | 340 | 520 | 60 | 60 | 60 |
| Startup cost (HOT) ($) | 4500 | 5000 | 550 | 560 | 900 | 170 | 260 | 30 | 30 | 30 |
| CST (h) | 5 | 5 | 4 | 4 | 4 | 2 | 2 | 0 | 0 | 0 |
| Initial status | 8 | 8 | -5 | -5 | -6 | -3 | -3 | -1 | -1 | -1 |
| Cost | | | | | | | | | | |
| $a_i$ | 0.00043 | 0.00063 | 0.00039 | 0.0007 | 0.0008 | 0.00056 | 0.00211 | 0.00480 | 0.10908 | 0.00951 |
| $b_i$ | 21.60 | 21.05 | 20.81 | 23.90 | 21.62 | 17.87 | 16.51 | 23.23 | 19.58 | 22.54 |
| $c_i$ | 958.20 | 1313.60 | 604.97 | 471.60 | 480.29 | 601.75 | 502.70 | 639.40 | 455.60 | 692.40 |
| $d_i$ | 450 | 600 | 320 | 260 | 280 | 310 | 300 | 340 | 270 | 380 |
| $e_i$ | 0.0410 | 0.0360 | 0.028 | 0.052 | 0.063 | 0.0480 | 0.0860 | 0.0820 | 0.0980 | 0.0943 |
| Mission | | | | | | | | | | |
| $\alpha_i$ | 10.33908 | 10.3390 | 30.03910 | 30.039 | 32.000 | 32.0000 | 033.000 | 033.0005 | 35.0005 | 36.00012 |
| $\beta_i$ | -0.24444 | -0.24444 | -0.40695 | -0.4069 | -0.3813 | -0.38132 | -0.39023 | -0.39023 | -0.39524 | -0.39864 |
| $\gamma_i$ | 0.00312 | 0.00312 | 0.00509 | 0.0050 | 0.0034 | 0.00344 | 0.00465 | 0.00465 | 0.00465 | 0.00470 |

For the studied power system, only the sources of emission are thermal units and the PV and wind farms are free of any emission. $E_u^k$ indicates per megawatt emission of a power plant unit at time $t$ which it includes $CO_2$, $SO_2$, and $NO_x$. The optimization algorithm should select operation points in such a way that the operating cost and emission are minimal [42–46].

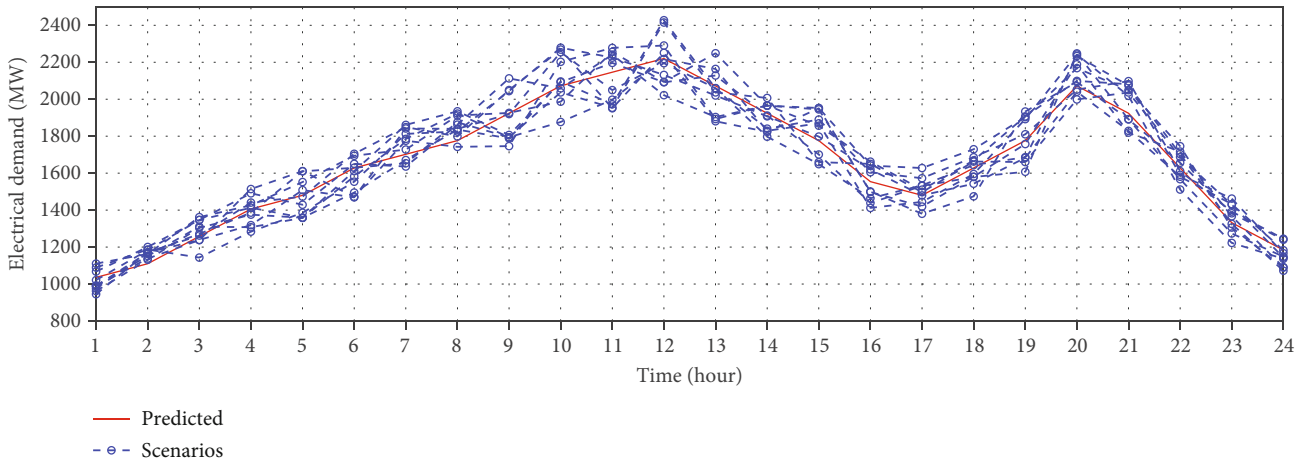


Figure 9: The predicted electrical demand for 24 hours.

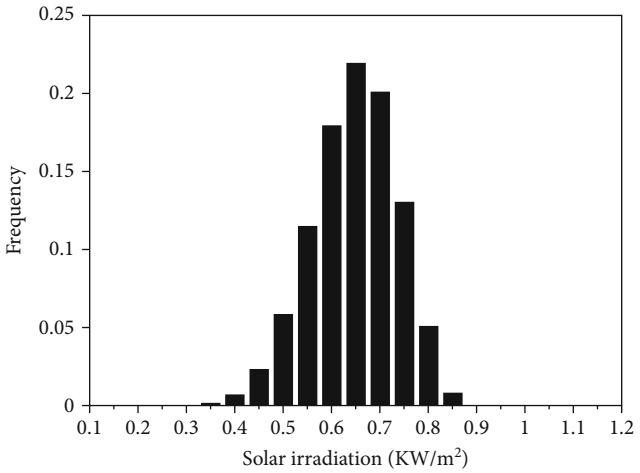


Figure 10: The solar irradiation PDF.

*2.4. Constraints.* The UC problem constraints are as follow:

*Power balance constraint*: the amount of electric power generation and consumption must be equal in every hour.

$$\sum_{k=1}^{N_u} P_u^k(t) + \sum_{j=1}^{N_{PV}} P_{PV}^j(t) + \sum_{i=1}^{N_{WT}} P_{WT}^i(t) = P_{\text{Load}}(t) + P_{\text{Loss}}(t) - P_{DR}(t). \tag{20}$$

*Thermal units' constraints*: the thermal units' constraints are as follows:

$$u^k P_u^{\text{Min}} \le P_u^k(t) \le u^k P_u^{\text{Max}} \tag{21}$$

$$P_u^k(t) - P_u^k(t-1) \le UR_u^{\text{Max}} \tag{22}$$

where $u^k$ is a binary number show unit status and UR is slope rate of production.

*Renewable farms constraints*: the generated power capacity of wind and PV are limited.

$$P_{WT}^{\text{Min}} \le P_{WT}^i(t) \le P_{WT}^{\text{Max}}, \tag{23}$$

$$P_{PV}^{\text{Min}} \le P_{PV}^j(t) \le P_{PV}^{\text{Max}}. \tag{24}$$

*Emission constraint*: the amount of emission produced by the thermal units should be less than the permissible limit.

$$\text{Emission}_u^k(t) \le E_u^{\text{Permit}}, \tag{25}$$

where $E_u^{\text{Permit}}$ is the maximum allowed amount of emission produced by the thermal unit.

## 3. Proposed Optimization Algorithm

To solve the UC problem and minimize of objective functions, a hybrid multiobjective grasshopper optimization algorithm and modified bald eagle search algorithm (MOGOA-MBES) are proposed. The performance of optimization algorithms is highly dependent on the parameters of the algorithm. If the algorithm parameters are not selected correctly, there is a possibility of nonconvergence or getting trapped at local optimal points. The velocity control parameters and scale control parameters have crucial role in MOGOA performance. The velocity control parameters include factors such as acceleration coefficient and time-varying coefficient. They influence the speed at which the grasshoppers move during the search. The scale control parameters include factors such as the scale change coefficient and scale change range. They are used to adjust the scale of position and velocity changes for the grasshoppers. Therefore, for the proposed algorithm, the parameters of the MOGOA are optimally selected by the modified version of the BES algorithm (MBES). So that in each iteration of the MOGOA algorithm, its parameters are optimally determined by the MBES. The mechanism of the proposed algorithm is shown in Figure 5.

As shown in Figure 5, the UC problem is solved using the MOGOA algorithm, and in each iteration, its parameters

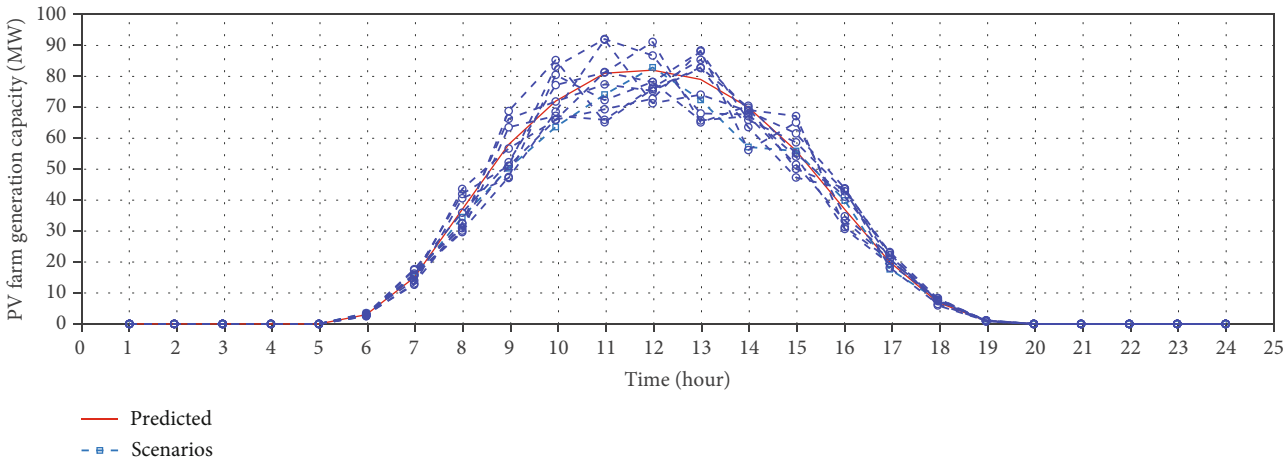


Figure 11: The PV farm generation capacity for the scenarios.

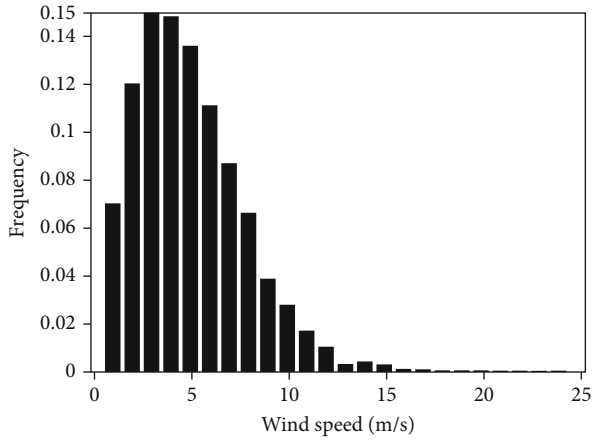


Figure 12: The wind speed PDF.

are optimized by the BES algorithm. Consequently, by precisely adjusting the parameters of the MOGOA algorithm through the BES algorithm, the best results will be obtained [47–51].

*3.1. Multiobjective GOA Algorithm.* The grasshopper optimization algorithm (GOA) is a particle-based metaheuristic algorithm which is modeled on the behavior of grasshopper. The effectiveness of the GOA has been proven in various articles, but in this paper, a modified version of the GOA algorithm is presented. The search method in the GOA consists of two parts: exploitation and exploration. For the exploration section, search agents are affected to move suddenly, while grasshoppers want to move locally. The swarming behavior of grasshoppers can be model as follows [52].

$$X_i = S_i + G_i + A_i, \tag{26}$$

where $X_i$ is the position of the $i$th particle, $S_i$ is the social interaction, $G_i$ is the gravitational force on the $i$th particle, and also $A_i$ is wind advection. Note that to avoid random behavior, this equation can be written as equation (21).

$$X_i = r_1 S_i + r_2 G_i + r_3 A_i, \tag{27}$$

where $r_1$, $r_2$, and $r_3$ are random numbers with uniform distribution in the range of (0, 1). The $S_i$ can be defended as

$$S_i = \sum_{\substack{j=1 \\ j \neq i}}^{N} s(d_{ij}) \widehat{d_{ij}}, \tag{28}$$

where $d_{ij} = |x_j - x_i|$ and $\widehat{d_{ij}} = (x_j - x_i)/d_{ij}$ are the distance and is unit vector between $i$th and $j$th grasshopper, respectively. Also, $s$ is a function to define the strength of social forces, which is calculated by

$$s(r) = f e^{-r/l} - e^{-r}, \tag{29}$$

where $f$ is the attraction intensity and $l$ is the attractive length scale. The gravitational force ($G_i$) can be calculated by

$$G_i = -g \widehat{e_g}, \tag{30}$$

where $g$ is the gravitational constant and $\widehat{e_g}$ represents a unit vector towards the center of the earth. Finally, the wind advection ($A_i$) is formulated as

$$A_i = u \widehat{e_w}, \tag{31}$$

where $u$ is a constant thrust and $\widehat{e_w}$ is a unit vector on the windward side. By substituting $S$, $G$, and $A$ in equation

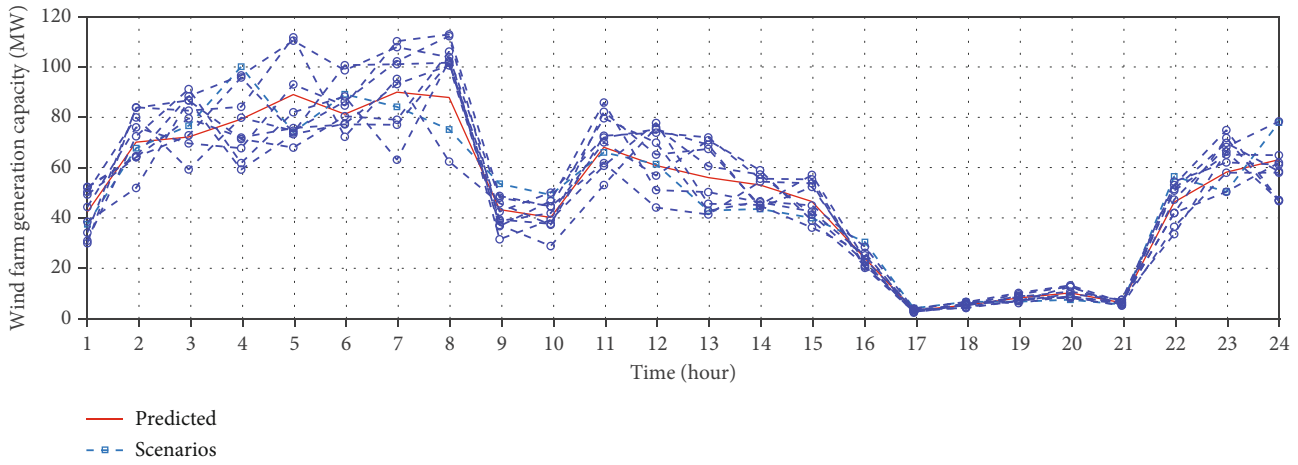


Figure 13: The wind farm generation capacity for the scenarios.

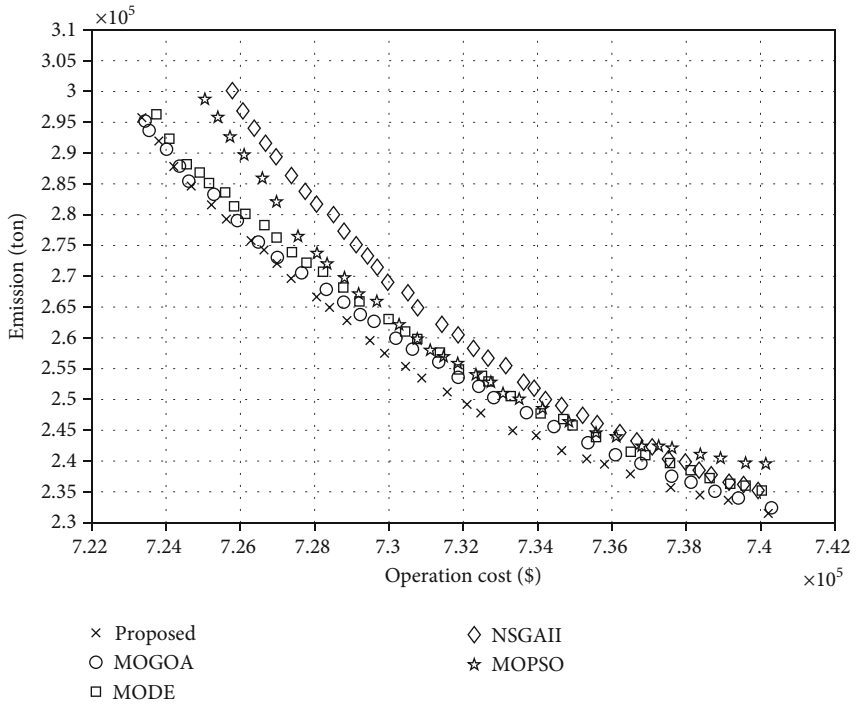


Figure 14: The Pareto front for the first part of simulation.

(21), this equation can be expanded as equation (32) [52]

$$X_i = \sum_{\substack{j=1 \\ j\neq i}}^{N} s\left(\left|x_j - x_i\right|\right) \frac{x_j - x_i}{d_{ij}} - g\widehat{e_g} + u\widehat{e_w}, \tag{32}$$

where $N$ is the number of the grasshoppers.

The multiobjective grasshopper optimization algorithm (MOGOA) is an extended version of the GOA algorithm, in which instead of an optimal solution, several optimal results will be created in the form of a Pareto front which are saved in the repository [53–57]. The archived results are updated by the Pareto front solutions, and finally, the MOGOA will select one of them from the repository. The main issue is to achieve a goal to increase the distribution of solutions in the archive. For this purpose, the number of neighboring results in the neighborhood of each result is selected by using a fixed interval, and the number of the neighboring results is calculated, and it is considered as a quantitative measure to evaluate the congestion of the area in the Pareto front. The probability the selected result from the repository is calculated by

$$P_i = \frac{1}{N_i}, \tag{33}$$

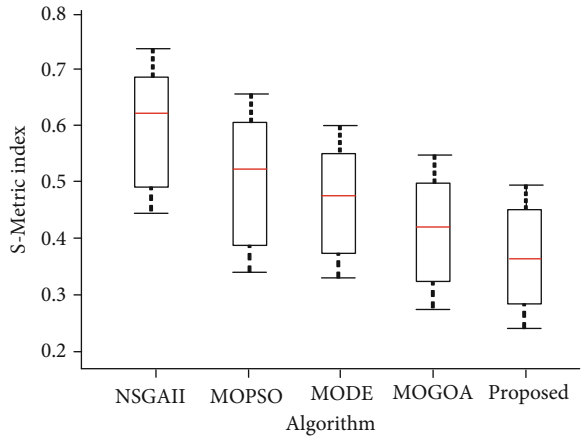


Figure 15: The S-metric index for the first part of simulation.

Table 2: The best results for the first part of the simulation.

| | NSGAII | MOPSO | MODE | MOGOA | Proposed |
|---|---|---|---|---|---|
| Cost ($) | 732614 | 732758 | 732608 | 732547 | 732318 |
| Emission (ton) | 256715 | 252804 | 252864 | 252097 | 249167 |

where $N_i$ is the number of the results in the neighboring of $i$ th results.

*3.2. Modified BES Algorithm.* The bald eagle search (BES) algorithm is a population-based intelligent optimization algorithm. Bald eagles often hunt from high altitudes, and they are able to track fish from long distances. Figure 6 shows bald eagles hunting. In order to find food, eagles choose an area with a certain capacity for fish and determine the route accordingly [58].

The BES algorithm to imitate the behavior of bald eagles is divided into three stages: space selection, search, and swooping. In the space selection stage, bald eagles choose the best place to search for prey in the search space and it is expressed as

$$P_{\text{new}}, i = P_{\text{best}} + \alpha \times r(P_{\text{mean}} - P_i), \tag{34}$$

where $r$ is a random number with uniform distribution, $\alpha$ is a number between 1.5 and 2, $P_{\text{best}}$ is the best region with high nutritional value, and $P_{\text{mean}}$ is the details of the previous step. Search spaces are selected close to each other in terms of food nature. The $\alpha$ parameter for the modified version of the BES algorithm is calculated by equation (35). This equation shows that the $\alpha$ is not constant, and it is dynamic. Choosing a dynamic coefficient for the $\alpha$ helps the algorithm determine the optimal value with higher accuracy.

$$\alpha = \alpha_0(1 + (ite_{\text{Max}} - ite)/ite_{\text{Max}}). \tag{35}$$

In the search stage, bald eagles move in a spiral direction in the search space and choose the best position to hunt prey. This feature enables the BES algorithm to discover new spaces and increase diversity. Figure 7 shows the search space stage.

The search space stage can be formulated by

$$Pi, \text{new} = \text{P}_i + \text{y}(i) \times (\text{P}_i - \text{P}_{i+1}) + x(i) \times (\text{P}_i - \text{P}_{\text{mean}}), \tag{36}$$

$$x(i) = \frac{xr(i)}{\max(|xr|)}, \tag{37}$$

$$y(i) = \frac{yr(i)}{\max(|yr|)}, \tag{38}$$

$$xr(i) = r(i) \times \sin(\theta(i)), \tag{39}$$

$$yr(i) = r(i) \times \cos(\theta(i)), \tag{40}$$

$$\theta(i) = a \times \pi \times \text{rand}, \tag{41}$$

$$r(i) = \theta(i) \times R \times \text{rand}, \tag{42}$$

where the parameter $a$ is between 5 and 10 and defines the point search angle. The $R$ is used to determine the number of cycles and is between 0.5 and 2. Finally, in the swooping stage, eagles dive from the best place towards their prey. Equations ((43)–(49)) formulate the swooping stage [58].

$$\begin{aligned} Pi, \text{new} = {} & \text{rand} \times P_{\text{best}} + x1(i) \times (\text{P}_i - \text{c1} \times \text{P}_{\text{mean}}) \\ & + \text{y1}(i) \times (\text{P}_i - \text{c2} \times \text{P}_{\text{best}}), \end{aligned} \tag{43}$$

$$x1(i) = \frac{xr(i)}{\max(|xr|)}, \tag{44}$$

$$y1(i) = \frac{yr(i)}{\max(|yr|)}, \tag{45}$$

$$xr(i) = r(i) \times \sinh[\theta(i))], \tag{46}$$

$$yr(i) = r(i) \times \cosh[\theta(i))], \tag{47}$$

$$\theta(i) = a \times \pi \times \text{rand}, \tag{48}$$

$$r(i) = \theta(i) \times R \times \text{rand}. \tag{49}$$

The eagle movement is plotted by a polar equation. Also, the best position can be found by multiplying the center point and current point division of polar for the $x$-axis and multiplying best point and current point division for the $y$ -axis. The parameters c1 and c2 increase the intensity of the eagle search movement [59–63]. The optimization result of the MBES algorithm on the benchmarks and comparing it with some other algorithms showed that the proposed MBES algorithm is more accurate than its previous version and other optimization algorithms.

*3.3. MOGOA-MBES.* The proposed algorithm is a combination of the multiobjective grasshopper algorithm (MOGOA) and the mutant version of the bald eagle search (MBES) algorithm. In the proposed hybrid algorithm, the parameters of the MOGOA ($f$, $l$, and $u$) are optimally estimated by the MBES algorithm in each iteration. The flowchart of the proposed MOGOA-MBES algorithm is shown in Figure 8.

The pseudo-code of the proposed MOGOA-MBES algorithm is given in Algorithm 1.

Table 3: The optimization results comparison for the first part of simulation.

| | NSGAII | MOPSO | MODE | MOGOA | Proposed |
|---|---|---|---|---|---|
| GD | 36217 | 33117 | 32457 | 31209 | 29882 |
| SM | 2921 | 2837 | 2741 | 2689 | 2653 |
| HV | 1.08344691e9 | 1. 06548738e9 | 0. 98569639e9 | 0. 93455681e9 | 0. 89339305e9 |

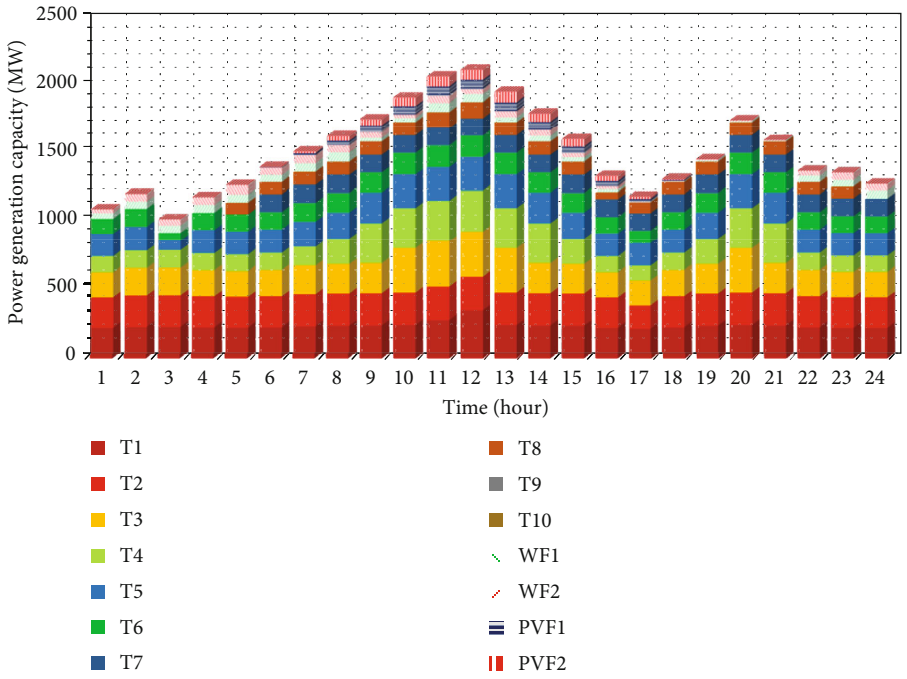


Figure 16: Production power of the units for the first part of the simulation.

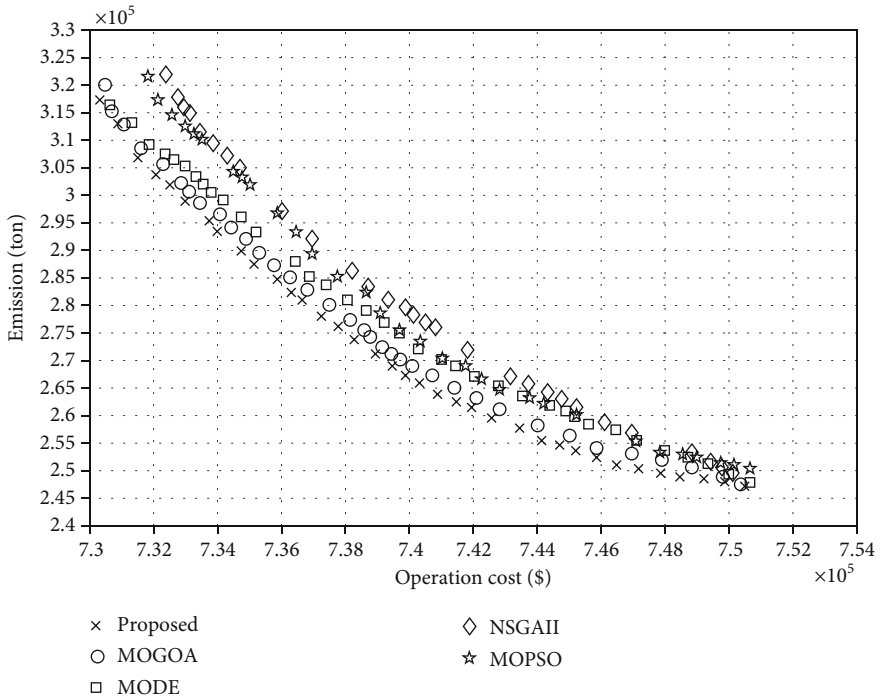


Figure 17: The Pareto front for the second part of simulation.

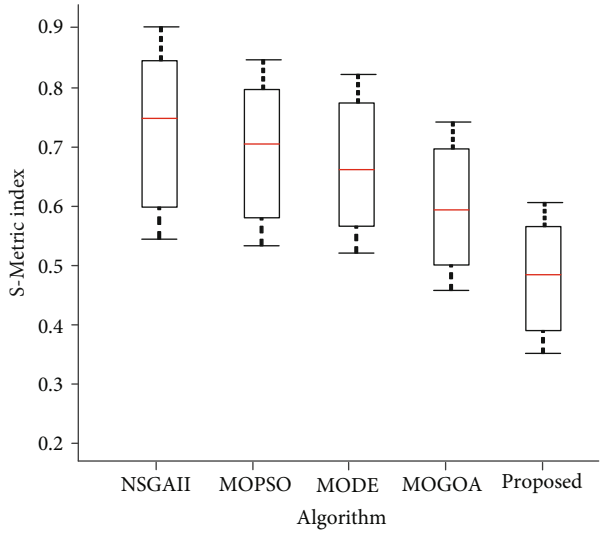


Figure 18: The S-Metric index for the second part of simulation.

Table 4: The best results for the second part of the simulation.

| | NSGAII | MOPSO | MODE | MOGOA | Proposed |
|---|---|---|---|---|---|
| Cost ($) | 742465 | 742314 | 742179 | 742148 | 741932 |
| Emission (ton) | 266401 | 266573 | 264146 | 263232 | 261097 |

## 4. Simulation Results and Discussion

In this section, first the studied power system and its parameters are introduced, and then the results of the proposed MOGOA-MBES are stated. Also, for better analysis of the results, the UC problem was also solved with multiobjective particle swarm optimization (MOPSO), nondominated sorting genetic algorithm (NSGAII), multiobjective differential evolution (MODE), and multiobjective grasshopper optimization algorithm (MOGOA). The population size and a maximum number of iterations are 100 and 50 for all the optimization algorithms, respectively. The maximum number of iterations is chosen in such a way to ensure that the algorithms have reached their final value.

*4.1. Introduction of the Case Study.* In this paper, a standard 10-unit power system with two wind farms, and two photovoltaic farms is selected for doing simulations. The 10-unit power system provides a simplified representation of a larger-scale power system. It strikes a balance between capturing essential system characteristics and keeping the model manageable and computationally feasible for analysis and optimization. The use of a standardized 10-unit power system facilitates benchmarking and comparison of different UC algorithms and methodologies. The cost and emission coefficients of the power system are given in Table 1. This table provides essential information about the operational characteristics, cost parameters, and emission coefficients of the units in the power system, which are crucial for performing unit commitment optimization in the UC problem. The G9 unit has a relatively high cost with a fuel cost coefficient, but it has the lowest startup costs (both cold and hot) compared to other units [64–68].

To perform simulation, 10 different scenarios were selected by the Monte Carlo Simulation (MCS) using demand and renewables sources PDFs. The predicted electrical demand for 24 hours in different scenarios is shown in Figure 9.

To model the solar irradiation intensity in the PV farm, the beta probability density function with coefficients $\alpha = 5.63$ and $\beta = 3.27$ is used [70]. In Figure 10, the beta PDF for solar radiation intensity is shown [71–75].

According to the beta PDF considered for the solar irradiation, the PV farm generation capacity for the scenarios is shown in Figure 11.

The wind speed in the studied power system has a Weibull probability density function with coefficients $k = 1.89$ and $c = 5.49$, similar to Figure 12.

According to the Weibull probability density function considered for wind speed and characteristics of wind turbines, the wind farm generation capacity for the selected scenarios by the MCS is shown in Figure 13.

*4.2. Scenarios Results Analysis.* The simulations are done in three sections. In the first section, the UC program is done in case of ignoring the uncertainties, and none of the loads are flexible. In the second part of the simulations, the uncertainties are considered in the UC program, and again, the flexible loads are omitted. Finally, in the third section, the UC program is carried out by considering the flexible loads in conditions of uncertainty.

*4.2.1. Without Uncertainty and Flexible Loads.* In the first part of the simulations, the UC program is done in the understudy power system in case of ignoring uncertainty and flexible loads. The electrical demand and the amount of wind and PV farm generation capacity for 24 hours are shown with a solid red line in Figures 9, 11, and 13, respectively. In Figure 14, the Pareto front of each optimization algorithm is shown for the first section of the simulation.

As shown in Figure 14, dominant results are uniformly distributed on the Pareto front. For a more accurate evaluation of the results, the S-metric index is calculated to determine the dispersion of dominant results, and it is shown by bar chart in Figure 15. Lower values of the average metric distance means that the Pareto responses were more dispersed, and zero value of the S-metric means that all the results are distributed in the Pareto front with almost the same distance.

The best solution should be chosen from the dominant particles. In this paper, the weighting method is used to select the final result. The values of the best results for optimization algorithms are given in Table 2.

According to the obtained accumulated in Table 2, the proposed MOGOA-MBES algorithm has performed better than other metaheuristic algorithms, and its cost and emission are the least. The final value of the operation cost is $732318, and the amount of emission is equal to 249167 tons. For better comparison, generational distance (GD), spacing metric (SM), and hypervolume (HV) for all the algorithms are calculated and accumulated in Table 3.

Table 5: The optimization results comparison for the second part of simulation.

| | NSGAII | MOPSO | MODE | MOGOA | Proposed |
|---|---|---|---|---|---|
| GD | 38055 | 37923 | 37679 | 37094 | 36784 |
| SM | 4027 | 3989 | 3925 | 3876 | 3816 |
| HV | 1.41558737e9 | 1.39856210e9 | 1.38976548e9 | 1.35482901e9 | 1.34194132e9 |

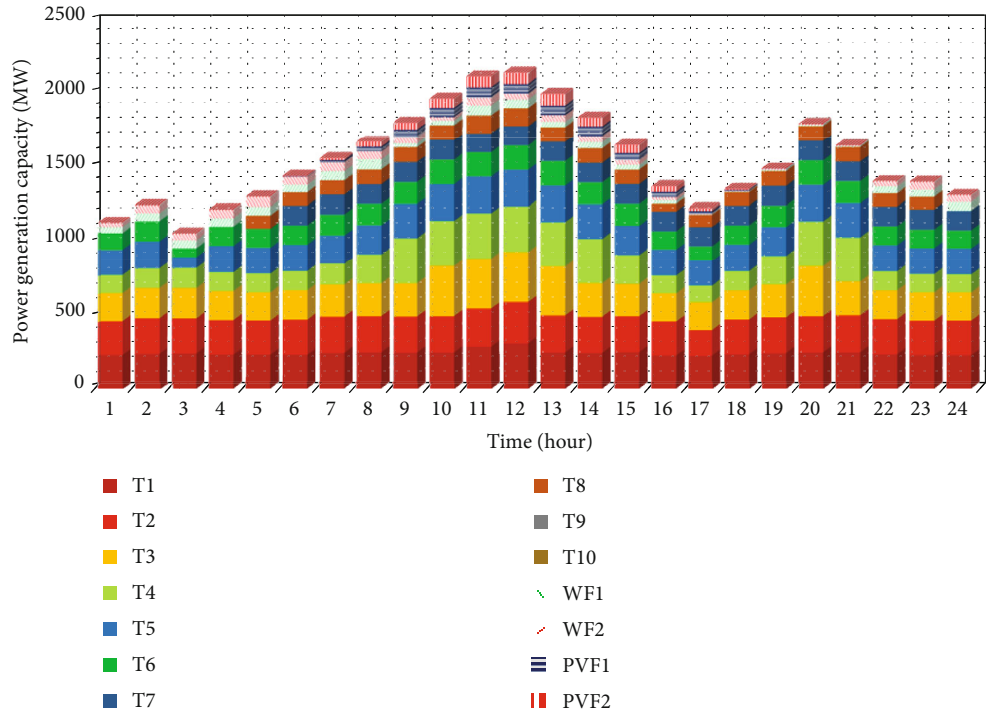


Figure 19: Production power of the units for the second part of the simulation.

In Figure 8, the production power of the power plants and renewable farms after optimization by the MOGOA-MBES is shown in Figure 16.

As shown in Figure 16, the thermal units T1 and T2 provided the largest share of the electrical demand. The wind and PV farms also participated in the UC program in the peak hours in order to reduce the operation cost and environmental emission by providing a part of the required electrical energy. Photovoltaic farms also had a great impact on reducing emissions and costs in the initial peak.

*4.2.2. Considering Uncertainty and without Flexible Loads.* In the second section of the simulation, the UC program is solved for the power system without flexible load and in the case of considering load and renewable generation uncertainties. The electrical demand and renewable farm generation capacity for different scenarios are shown by dashed line in Figures 9, 11, and 13, respectively. In Figure 17, the values of dominant particles for the second section are shown.

For better analysis of the optimization results, the S-metric index is calculated for the algorithms, and it is shown in Figure 18.

According to the S-metric results, the dispersion of the dominant particles has increased compared to the first scenario, and the reason is the consideration of uncertainty. The S-metric average for the proposed MOGOA-MBES algorithm is about 0.48 p.u. which is lower than other metaheuristic algorithms. Conversely, the S-metric average for the NSGAII algorithm is more than all the algorithms, which confirms the high dispersion of the obtained results by this algorithm.

The operation cost and emission values of the final optimal results selected by the weighting method from the dominant results are given in Table 4.

According to the Table 3 results, the lowest operation cost and emission are related to the proposed MOGOA-MBES algorithm, which are $741932 and 261097 ton, respectively. While the highest cost is related to the NSGAII algorithm which is equal to $742465, and the highest amount of emission is related to the MOPSO algorithm which is equal to 266573 ton. The GD, SM, and HV indexes for all the algorithms in the second part of the simulation are given in Table 5.

In Figure 19, the electric power produced by the thermal units and renewable farms, in the case of solving the UC problem with the proposed MOGOA-MBES algorithm, is shown by a bar chart.

In this section, the thermal unit Th1 supplies about 14.23% of the electrical energy demand, which is more than other generation units. The wind farms provide about 5.2% and the photovoltaic farms provide about 4.3% of the electrical load in the power system. The production power of wind

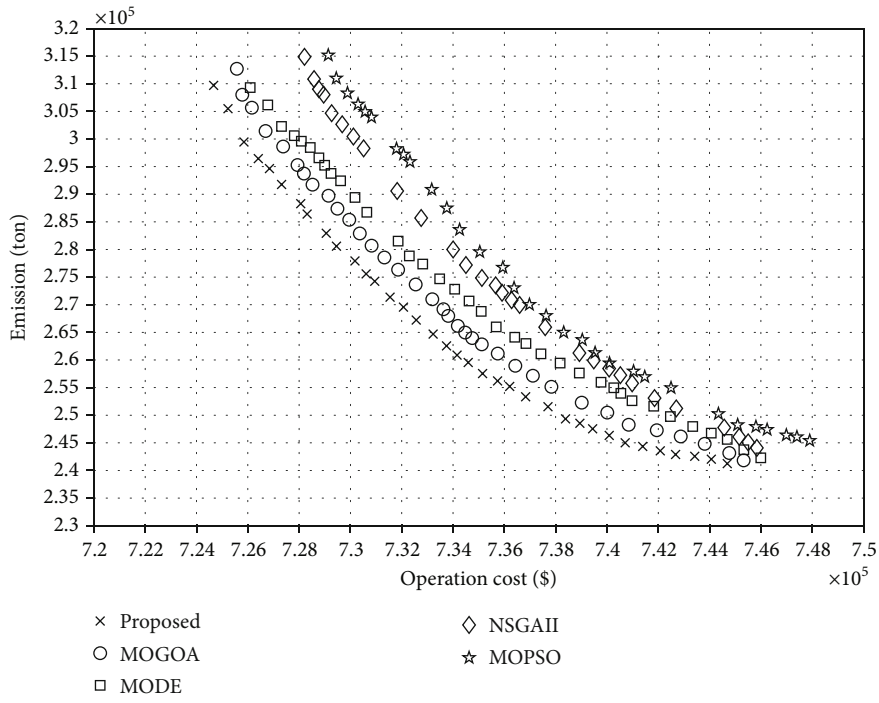


Figure 20: The Pareto front for the third part of simulation.

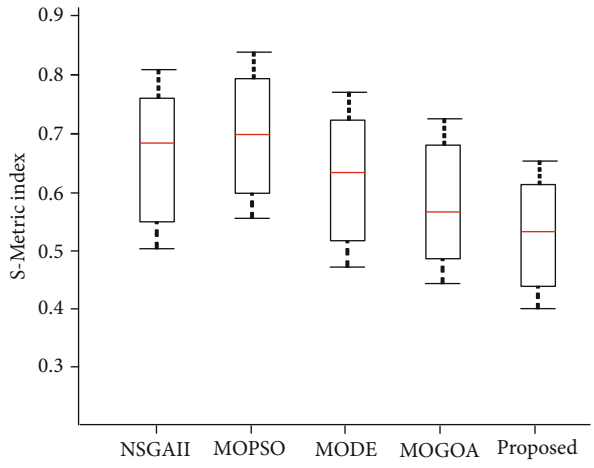


Figure 21: The S-metric index for the third part of the simulation.

and PV farms is often focused on the peak load times of the network.

*4.2.3. Considering Uncertainty and Using Flexible Loads.* Finally, for the third part of the simulations, the uncertainties and flexible loads are considered in the UC program. Therefore, the electrical demand can be reduced by the flexible loads in some hours to help the power system. The electrical demand and renewable generation capacities are considered similar to the second section. In Figure 20, the Pareto front obtained by multiobjective optimization algorithms is shown.

Table 6: The best results for the third part of the simulation.

| | NSGAII | MOPSO | MODE | MOGOA | Proposed |
|---|---|---|---|---|---|
| Cost ($) | 739804 | 739447 | 737738 | 737236 | 736849 |
| Emission (ton) | 264856 | 262409 | 260349 | 258507 | 257381 |

Also, the S-metric index is calculated to determine the dispersion of dominant results in the third section, and it is displayed in Figure 21.

The best result for the third section is also selected by the weighting method, and it is accumulated in Table 6.

The results of this section of simulation show that the participation of flexible loads in the UC program has reduced the operation cost in the conditions of uncertainties. As a result, demand reduction during peak hours reduces operation cost and emission even when uncertainties are taken into account. Also, similar to previous sections, the proposed MOGOA-MBES has better performance than other algorithms. The power system operation cost and emission are $736480 and 255890 tons after doing optimization by the MOGOA-MBES. The GD, SM, and HV indexes for the third part of the simulation are accumulated in Table 7.

In Figure 22, the contribution of the thermal units and renewable farms to total electrical demand is shown.

As shown in Figure 22, electrical energy consumption is decreased during peak hours due to flexible load participation in the UC program. Also, the thermal units Th1 and Th2 provided 40% of the total electrical energy demand. Wind farms and photovoltaic farms provided about 5% of

Table 7: The optimization results comparison for the third part of simulation.

| | NSGAII | MOPSO | MODE | MOGOA | Proposed |
|---|---|---|---|---|---|
| GD | 37594 | 370677 | 36280 | 35319 | 34583 |
| SM | 3476 | 3346 | 3169 | 2947 | 2893 |
| HV | 1.23678509e9 | 1.15683722e9 | 1.10985237e9 | 1.09844621e9 | 1.01985934e9 |

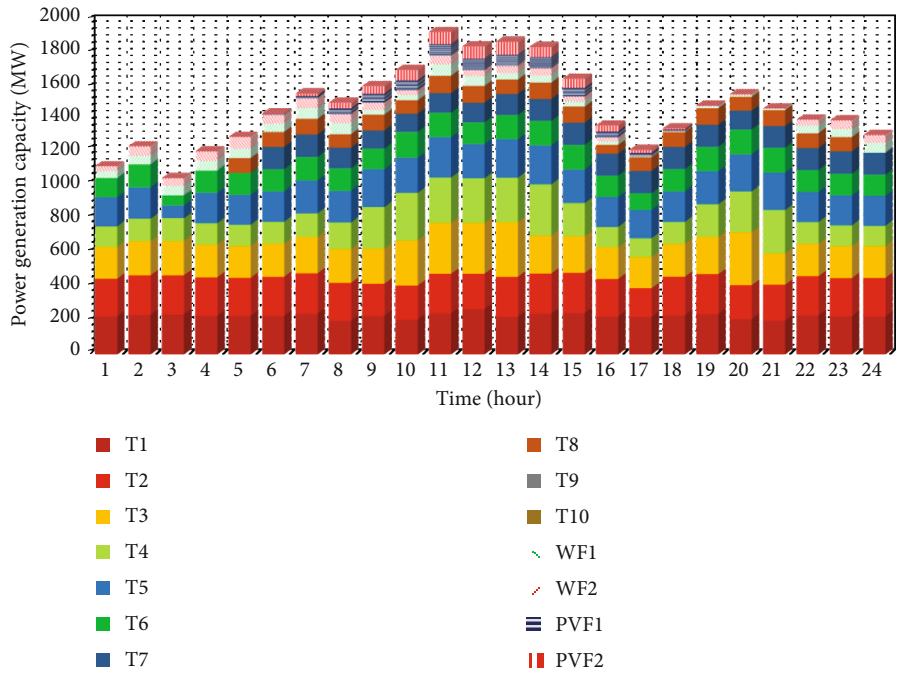


Figure 22: Production power of the units for the third part of the simulation.

the total load. Supplying power by renewable operation cost and emission reduction.

## 5. Conclusion

In this paper, the optimal stochastic planning of resources in the power system with thermal units in the presence of wind farms and photovoltaics has been done with the approach of reducing operating costs and environmental pollution. In the studies, the uncertainties of electric loads and the uncertainties of the production power of renewable resources are considered. It is also assumed that the loads are flexible and have the ability to participate in the electrical and thermal load response program. A hybrid self-adjusting algorithm was proposed, which has the capability of extensive search of the search space and does not get trapped in local optimal points. The optimization results in three parts showed that the proposed MOGOA-MBES algorithm was more accurate than other multiobjective metaheuristic algorithms. Also, the results proved that when the uncertainties in the participation of the units were considered, the cost and pollution increased, but if there are responsive loads in the power system and they participate in the load response program, the cost and pollution are about 3%. Will be reduced. In the recent decade, photovoltaic and wind renewable resources have been extensively deployed in power systems, which can have a direct impact on UC studies. In this context, providing an accurate model of the power system under uncertain conditions is of great importance. This paper simulation results can be used in the real world. In line with the research carried out in this article, it is possible to consider the issue of rotating reservation and pump storage.

## Data Availability

The data used to support the findings of this study are included within the paper.

## Conflicts of Interest

The authors declare that they have no conflicts of interest.

## References

[1] F. Ioannidis, K. Kosmidou, I. Kalaitzoglou, K. Andriosopoulos, and E. Galariotis, "Investing in bridging fuels: the unit commitment problem of public vs. private ventures," *The Energy Journal*, vol. 44, no. 1, 2023.

[2] H. Shokouhandeh, M. Ahmadi Kamarposhti, I. Colak, and K. Eguchi, "Unit commitment for power generation systems based on prices in smart grid environment considering uncertainty," *Sustainability*, vol. 13, no. 18, article 10219, 2021.

[3] H. Abdi, "Profit-based unit commitment problem: a review of models, methods, challenges, and future directions," *Renewable and Sustainable Energy Reviews*, vol. 138, article 110504, 2021.

[4] S. Wang, N. Zheng, C. D. Bothwell, Q. Xu, S. Kasina, and B. F. Hobbs, "Crediting variable renewable energy and energy storage in capacity markets: effects of unit commitment and storage operation," *IEEE Transactions on Power Systems*, vol. 37, no. 1, pp. 617–628, 2022.

[5] F. Fallahi and P. Maghouli, "Integrated unit commitment and natural gas network operational planning under renewable generation uncertainty," *International Journal of Electrical Power & Energy Systems*, vol. 117, article 105647, 2020.

[6] S. Tiwari, B. Dwivedi, M. P. Dave, A. Shrivastava, A. Agrawal, and V. S. Bhadoria, "Unit commitment problem in renewable integrated environment with storage: a review," *International Transactions on Electrical Energy Systems*, vol. 31, no. 10, article e12775, 2021.

[7] Y. Y. Hong and G. F. D. Apolinario, "Uncertainty in unit commitment in power systems: a review of models, methods, and applications," *Energies*, vol. 14, no. 20, p. 6658, 2021.

[8] M. Pluta, A. Wyrwa, W. Suwała, J. Zyśk, M. Raczyński, and S. Tokarski, "A generalized unit commitment and economic dispatch approach for analysing the Polish power system under high renewable penetration," *Energies*, vol. 13, no. 8, p. 1952, 2020.

[9] D. Yang, X. Zhou, Z. Yang, Y. Guo, and Q. Niu, "Low carbon multi-objective unit commitment integrating renewable generations," *IEEE Access*, vol. 8, pp. 207768–207778, 2020.

[10] T. Anbazhagi, K. Asokan, and R. AshokKumar, "A mutual approach for profit-based unit commitment in deregulated power system integrated with renewable energy sources," *Transactions of the Institute of Measurement and Control*, vol. 43, no. 5, pp. 1102–1116, 2021.

[11] B. H. Brito, E. C. Finardi, and F. Y. K. Takigawa, "Mixed-integer nonseparable piecewise linear models for the hydropower production function in the unit commitment problem," *Electric Power Systems Research*, vol. 182, article 106234, 2020.

[12] M. Håberg, "Fundamentals and recent developments in stochastic unit commitment," *International Journal of Electrical Power & Energy Systems*, vol. 109, pp. 38–48, 2019.

[13] J. Zhao, S. Liu, M. Zhou, X. Guo, and L. Qi, "An improved binary cuckoo search algorithm for solving unit commitment problems: methodological description," *IEEE Access*, vol. 6, pp. 43535–43545, 2018.

[14] F. Li, J. Qin, and W. X. Zheng, "Distributed Q-learning-based online optimization algorithm for unit commitment and dispatch in smart grid," *IEEE Transactions on Cybernetics*, vol. 50, no. 9, pp. 4146–4156, 2020.

[15] K. S. Reddy, L. Panwar, B. K. Panigrahi, and R. Kumar, "Binary whale optimization algorithm: a new metaheuristic approach for profit-based unit commitment problems in competitive electricity markets," *Engineering Optimization*, vol. 51, no. 3, pp. 369–389, 2019.

[16] Y. Yang, J. C. H. Peng, C. Ye, Z. S. Ye, and Y. Ding, "A criterion and stochastic unit commitment towards frequency resilience of power systems," *IEEE Transactions on Power Systems*, vol. 37, no. 1, pp. 640–652, 2022.

[17] J. Huotari, A. Ritari, J. Vepsäläinen, and K. Tammi, "Hybrid ship unit commitment with demand prediction and model predictive control," *Energies*, vol. 13, no. 18, p. 4748, 2020.

[18] N. Yang, Z. Dong, L. Wu et al., "A comprehensive review of security-constrained unit commitment," *Journal of Modern Power Systems and Clean Energy*, vol. 10, no. 3, pp. 562–576, 2022.

[19] A. Esmaeily, A. Ahmadi, F. Raeisi, M. R. Ahmadi, A. E. Nezhad, and M. Janghorbani, "Evaluating the effectiveness of mixed-integer linear programming for day-ahead hydrothermal self-scheduling considering price uncertainty and forced outage rate," *Energy*, vol. 122, pp. 182–193, 2017.

[20] J. Wang, M. Guo, and Y. Liu, "Hydropower unit commitment with nonlinearity decoupled from mixed integer nonlinear problem," *Energy*, vol. 150, pp. 839–846, 2018.

[21] J. Zou, S. Ahmed, and X. A. Sun, "Multistage stochastic unit commitment using stochastic dual dynamic integer programming," *IEEE Transactions on Power Systems*, vol. 34, no. 3, pp. 1814–1823, 2019.

[22] B. Fu, C. Ouyang, C. Li, J. Wang, and E. Gul, "An improved mixed integer linear programming approach based on symmetry diminishing for unit commitment of hybrid power system," *Energies*, vol. 12, no. 5, p. 833, 2019.

[23] Z. K. Feng, W. J. Niu, W. C. Wang, J. Z. Zhou, and C. T. Cheng, "A mixed integer linear programming model for unit commitment of thermal plants with peak shaving operation aspect in regional power grid lack of flexible hydropower energy," *Energy*, vol. 175, pp. 618–629, 2019.

[24] V. Kumar and D. Kumar, "Binary whale optimization algorithm and its application to unit commitment problem," *Neural Computing and Applications*, vol. 32, no. 7, pp. 2095–2123, 2020.

[25] R. Ponciroli, N. E. Stauff, J. Ramsey, F. Ganda, and R. B. Vilim, "An improved genetic algorithm approach to the unit commitment/economic dispatch problem," *IEEE Transactions on Power Systems*, vol. 35, no. 5, pp. 4005–4013, 2020.

[26] Y. Zhai, X. Liao, N. Mu, and J. Le, "A two-layer algorithm based on PSO for solving unit commitment problem," *Soft Computing*, vol. 24, no. 12, pp. 9161–9178, 2020.

[27] L. K. Panwar, S. Reddy, A. Verma, B. K. Panigrahi, and R. Kumar, "Binary grey wolf optimizer for large scale unit commitment problem," *Swarm and Evolutionary Computation*, vol. 38, pp. 251–266, 2018.

[28] P. Nikolaidis and S. Chatzis, "Gaussian process-based Bayesian optimization for data-driven unit commitment," *International Journal of Electrical Power & Energy Systems*, vol. 130, article 106930, 2021.

[29] J. Chen, F. Luo, G. Li, and Z. Wang, "Batch Bayesian optimization with adaptive batch acquisition functions via multi-objective optimization," *Swarm and Evolutionary Computation*, vol. 79, article 101293, 2023.

[30] T. C. Bora, V. C. Mariani, and L. dos Santos Coelho, "Multi-objective optimization of the environmental-economic dispatch with reinforcement learning based on non-dominated sorting genetic algorithm," *Applied Thermal Engineering*, vol. 146, pp. 688–700, 2019.

[31] J. S. Pan, P. Hu, and S. C. Chu, "Binary fish migration optimization for solving unit commitment," *Energy*, vol. 226, article 120329, 2021.

[32] A. Singh and A. Khamparia, "A hybrid whale optimization-differential evolution and genetic algorithm based approach to solve unit commitment scheduling problem: WODEGA," *Sustainable Computing: Informatics and Systems*, vol. 28, article 100442, 2020.

[33] H. O. R. Howlader, M. M. Sediqi, A. M. Ibrahimi, and T. Senjyu, "Optimal thermal unit commitment for solving duck curve problem by introducing CSP, PSH and demand response," *IEEE Access*, vol. 6, pp. 4834–4844, 2018.

[34] D. Madzharov, E. Delarue, and W. D'haeseleer, "Integrating electric vehicles as flexible load in unit commitment modeling," *Energy*, vol. 65, pp. 285–294, 2014.

[35] F. Jabari, M. Mohammadpourfard, and B. Mohammadi-Ivatloo, "Implementation of demand response programs on unit commitment problem," in *Demand Response Application in Smart Grids*, pp. 37–54, Springer, Cham, 2020.

[36] S. P. Roukerd, A. Abdollahi, and M. Rashidinejad, "Uncertainty-based unit commitment and construction in the presence of fast ramp units and energy storages as flexible resources considering enigmatic demand elasticity," *Journal of Energy Storage*, vol. 29, article 101290, 2020.

[37] S. Rajamand, "Effect of demand response program of loads in cost optimization of microgrid considering uncertain parameters in PV/WT, market price and load demand," *Energy*, vol. 194, article 116917, 2020.

[38] K. Qing, Q. Huang, Y. Du, L. Jiang, O. Bamisile, and W. Hu, "Distributionally robust unit commitment with an adjustable uncertainty set and dynamic demand response," *Energy*, vol. 262, article 125434, 2023.

[39] A. Sayed, M. Ebeed, Z. M. Ali et al., "A hybrid optimization algorithm for solving of the unit commitment problem considering uncertainty of the load demand," *Energies*, vol. 14, no. 23, p. 8014, 2021.

[40] H. Shokouhandeh and M. Jazaeri, "An enhanced and autotuned power system stabilizer based on optimized interval type-2 fuzzy PID scheme," *International Transactions on Electrical Energy Systems*, vol. 28, no. 1, p. e2469, 2018.

[41] H. Shokouhandeh and M. Jazaeri, "Robust design of fuzzy-based power system stabiliser considering uncertainties of loading conditions and transmission line parameters," *IET Generation, Transmission & Distribution*, vol. 13, no. 19, pp. 4287–4300, 2019.

[42] Y. Liu and K. Xu, "Millimeter-wave bandpass filters using on-chip dual-mode resonators in 0.13-$\mu$m SiGe BiCMOS technology," *IEEE Transactions on Microwave Theory and Techniques*, pp. 1–11, 2023.

[43] K. Xu and Y. Liu, "Millimeter-wave on-Chip bandpass filter using complementary-broadside-coupled structure," *IEEE Transactions on Circuits and Systems II: Express Briefs*, p. 1, 2023.

[44] D. Wang, K. D. Xu, S. Luo, Y. Cui, L. Zhang, and J. Cui, "A high Q-factor dual-band terahertz metamaterial absorber and its sensing characteristics," *Nanoscale*, vol. 15, no. 7, pp. 3398–3407, 2023.

[45] B. Sun, Y. Li, Y. Zeng, J. Chen, and J. Shi, "Optimization planning method of distributed generation based on steady-state security region of distribution network," *Energy Reports*, vol. 8, pp. 4209–4222, 2022.

[46] Z. Huang, T. Li, K. Huang, H. Ke, M. Lin, and Q. Wang, "Predictions of flow and temperature fields in a T-junction based on dynamic mode decomposition and deep learning," *Energy*, vol. 261, article 125228, 2022.

[47] P. Wang, P. Yu, J. Lu, and Y. Zhang, "The mediation effect of land surface temperature in the relationship between land use-cover change and energy consumption under seasonal variations," *Journal of Cleaner Production*, vol. 340, article 130804, 2022.

[48] X. Lin, R. Yu, J. Yu, and H. Wen, "Constant coupling effect-based PLL for synchronization stability enhancement of grid-connected converter under weak grids," *IEEE Transactions on Industrial Electronics*, vol. 70, no. 11, pp. 11310–11323, 2023.

[49] Z. Yan and H. Wen, "Electricity theft detection base on extreme gradient boosting in AMI," *IEEE Transactions on Instrumentation and Measurement*, vol. 70, pp. 1–9, 2021.

[50] J. Song, A. Mingotti, J. Zhang, L. Peretto, and H. Wen, "Fast iterative-interpolated DFT phasor estimator considering out-of-band interference," *IEEE Transactions on Instrumentation and Measurement*, vol. 71, pp. 1–14, 2022.

[51] Y. Gao, M. Doppelbauer, J. Ou, and R. Qu, "Design of a double-side flux modulation permanent magnet machine for servo application," *IEEE Journal of Emerging and Selected Topics in Power Electronics*, vol. 10, no. 2, pp. 1671–1682, 2022.

[52] S. Saremi, S. Mirjalili, and A. Lewis, "Grasshopper optimisation algorithm: theory and application," *Advances in Engineering Software*, vol. 105, pp. 30–47, 2017.

[53] B. Shao, Q. Xiao, L. Xiong et al., "Power coupling analysis and improved decoupling control for the VSC connected to a weak AC grid," *International Journal of Electrical Power & Energy Systems*, vol. 145, article 108645, 2023.

[54] C. Chen, X. Wu, X. Yuan, and X. Zheng, "A new technique for the subdomain method in predicting electromagnetic performance of surface-mounted permanent magnet motors with shaped magnets and a quasi-regular polygon rotor Core," *IEEE Transactions on Energy Conversion*, vol. 38, no. 2, pp. 1396–1409, 2023.

[55] S. Liu, Z. Song, Z. Dong, Y. Liu, and C. Liu, "Generic carrier-based PWM solution for series-end winding PMSM traction system with adaptative overmodulation scheme," *IEEE Transactions on Transportation Electrification*, vol. 9, no. 1, pp. 712–726, 2023.

[56] H. Tang, J. Di, Z. Wu, and W. Li, "Temperature analysis for the asymmetric six-phase permanent magnet synchronous motor in healthy and fault-tolerant modes," *IEEE Transactions on Industrial Electronics*, vol. 70, no. 7, pp. 6482–6493, 2023.

[57] S. Liu, Z. Song, Y. Liu, Y. Chen, and C. Liu, "Flux-weakening controller design of dual three-phase PMSM drive system with copper loss minimization," *IEEE Transactions on Power Electronics*, vol. 38, no. 2, pp. 2351–2363, 2023.

[58] H. A. Alsattar, A. A. Zaidan, and B. B. Zaidan, "Novel meta-heuristic bald eagle search optimisation algorithm," *Artificial Intelligence Review*, vol. 53, no. 3, pp. 2237–2264, 2020.

[59] S. Liu and C. Liu, "Virtual-vector-based robust predictive current control for dual three-phase PMSM," *IEEE Transactions on Industrial Electronics*, vol. 68, no. 3, pp. 2048–2058, 2021.

[60] S. Liu and C. Liu, "Direct harmonic current control scheme for dual three-phase PMSM drive system," *IEEE Transactions on Power Electronics*, vol. 36, no. 10, pp. 11647–11657, 2021.

[61] S. Liu, C. Liu, H. Zhao, Y. Liu, and Z. Dong, "Improved flux weakening control strategy for five-phase PMSM considering harmonic voltage vectors," *IEEE Transactions on Power Electronics*, vol. 37, no. 9, pp. 10967–10980, 2022.

[62] K. Liao, B. Pang, J. Yang, and Z. He, "Compensation strategy of wideband voltage harmonics for doubly-fed induction generator," *IEEE Transactions on Energy Conversion*, vol. 38, no. 1, pp. 674–684, 2023.

[63] K. Liao, D. Lu, M. Wang, and J. Yang, "A low-pass virtual filter for output power smoothing of wind energy conversion

systems," *IEEE Transactions on Industrial Electronics*, vol. 69, no. 12, pp. 12874–12885, 2022.

[64] J. Liang, B. Kato, and Y. Wang, "Constructing simplified models for dynamic analysis of monopile-supported offshore wind turbines," *Ocean Engineering*, vol. 271, article 113785, 2023.

[65] Y. Duan, Y. Zhao, and J. Hu, "An initialization-free distributed algorithm for dynamic economic dispatch problems in microgrid: modeling, optimization and analysis," *Sustainable Energy, Grids and Networks*, vol. 34, article 101004, 2023.

[66] A. Taghieh, A. Mohammadzadeh, C. Zhang, N. Kausar, and O. Castillo, "A type-3 fuzzy control for current sharing and voltage balancing in microgrids," *Applied Soft Computing*, vol. 129, article 109636, 2022.

[67] L. Lin, J. Shi, C. Ma et al., "Non-intrusive residential electricity load decomposition via low-resource model transferring," *Journal of Building Engineering*, vol. 73, article 106799, 2023.

[68] N. Huang, Q. Chen, G. Cai, D. Xu, L. Zhang, and W. Zhao, "Fault diagnosis of bearing in wind turbine gearbox under actual operating conditions driven by limited data with noise labels," *IEEE Transactions on Instrumentation and Measurement*, vol. 70, pp. 1–10, 2021.

[69] Y. Zhang, K. Liu, X. Liao, L. Qin, and X. An, "Stochastic dynamic economic emission dispatch with unit commitment problem considering wind power integration," *International Transactions on Electrical Energy Systems*, vol. 28, no. 1, article e2472, 2018.

[70] S. Xu, W. Huang, D. Huang et al., "A reduced-order observer-based method for simultaneous diagnosis of open-switch and current sensor faults of a grid-tied NPC inverter," *IEEE Transactions on Power Electronics*, vol. 38, no. 7, pp. 9019–9032, 2023.

[71] J. Gao, H. Sun, J. Han, Q. Sun, and T. Zhong, "Research on recognition method of electrical components based on FEYOLOv4-tiny," *Journal of Electrical Engineering & Technology*, vol. 17, pp. 3541–3551, 2022.

[72] W. Dang, S. Liao, B. Yang et al., "An encoder-decoder fusion battery life prediction method based on Gaussian process regression and improvement," *Journal of Energy Storage*, vol. 59, article 106469, 2023.

[73] J. Wang, J. Tian, X. Zhang et al., "Control of time delay force feedback teleoperation system with finite time convergence," *Frontiers in Neurorobotics*, vol. 16, 2022.

[74] Q. Gu, J. Tian, B. Yang et al., "A novel architecture of a six degrees of freedom parallel platform," *Electronics*, vol. 12, no. 8, p. 1774, 2023.

[75] B. Cao, W. Dong, Z. Lv, Y. Gu, S. Singh, and P. Kumar, "Hybrid microgrid many-objective sizing optimization with fuzzy decision," *IEEE Transactions on Fuzzy Systems*, vol. 28, no. 11, pp. 2702–2710, 2020.